On-target diagnosing of few-cycle pulses by high-order-harmonic generation

Danilo S. Brambila, Anton Husakou, Misha Ivanov, and Nickolai Zhavoronkov*
Max Born Institute, Max Born Straße 2a, 12489 Berlin, Germany
(Received 27 January 2017; published 18 December 2017)

We propose an approach to determine the residual phase distortion directly in the interaction region of few-cycle laser radiation with a gaseous target. We describe how the spectra of the generated high harmonics measured as a function of externally introduced dispersion into the driving few-cycle laser pulse can be used to decode small amounts of second- and third-order spectral phase, including the sign. The diagnosis is based on the analysis of several key features in the high-harmonic spectrum: the depth of spectral modulation, the position of the cutoff, and the symmetry of the spectrum with respect to the introduced dispersion. The approach is applicable to pulses without carrier-envelope phase (CEP) stabilization. Surprisingly, we find that for nearly-single-cycle pulses with nonstabilized CEP, deep spectral modulations in the harmonic spectra emerge for positively rather than negatively chirped pulses, in contrast to the case of CEP-stabilized pulses.

DOI: 10.1103/PhysRevA.96.063825

I. INTRODUCTION

High harmonic generation (HHG) is the enabling technology for table-top sources of bright coherent extreme ultraviolet (XUV) and soft x-ray radiation in a form of isolated attosecond pulses and attosecond pulse trains. High temporal resolution at the level of a few tens of attoseconds is achieved thanks to the highly nonlinear nature of the harmonic response, which makes it very sensitive to the sub-cycle behavior of the driving laser field [1–5]. For few-cycle laser pulses, this sensitivity of the harmonic response to the pulse parameters, especially the carrier-envelope phase (CEP), is not only crucial for generation of attosecond pulses [6], but has also been used to measure the CEP of the driving pulse [1]. Large spectral bandwidth of nearly single-cycle pulses makes them very susceptible to dispersion-induced distortions during propagation, be it a few tens of centimeters of the air or an additional mirror reflection. However, precise information on parameters of such extremely short pulses, directly at the micrometer-sized target, is crucial for a correct interpretation of experimental data. Several elegant techniques proposed to address this problem are based on perturbation of the electron trajectory during high harmonic generation by an additional weak field and the analysis of the generated harmonic spectrum [7–9]. None of these methods work for pulses without CEP stabilization.

Here we introduce what we believe is a very distinct alternative and/or complementary approach, focusing on pulses without CEP stabilization. We refer to it as high-harmonic-generation dispersion scan (HHG D-scan). Our methodology is based on analysis of the HHG spectra upon introduction of a controllable amount of dispersion to the driving few-cycle laser pulse. We demonstrate, that even for pulses without CEP stabilization, HHG spectra can offer a very sensitive tool for detecting small quadratic (β) and third-order (γ) spectral phases *in situ*. An attractive feature of the proposed approach lies in the straightforward identification of quadratic and cubic spectral phases in the dispersion-dependent harmonic spectrum, as discussed below.

Below we demonstrate the following: First, near the cutoff of the harmonic spectra, the relative phase between adjacent attosecond bursts generated by pulses with $\beta > 0$ is considerably less sensitive to variations of the carrier-envelope phase than for the $\beta < 0$. Second, variation of the spectral cutoff is sensitive to the sign of the third-order phase, distinguishing negative γ from positive. Third, introducing additional controlled variation of β and γ allows one to characterize the sign and the amount of small second-order and third-order spectral phases of the original incident pulse direct in the interaction region. Our approach can be viewed as a highly nonlinear version of the D-scan method of pulse characterization [10,11]. However, similarities are only limited to the working concept, since the analysis of the recorded XUV spectra is completely different.

The high-harmonic spectrum as a function of externally introduced dispersion forms a two-dimensional spectrogram. Our analysis shows that second- and third-order spectral phases are responsible for two distinct features of these spectrograms: the depth of the spectral modulation and the asymmetry of the cutoff. While we expect that fourth- and higher-order spectral phases can be also extracted based on the properties of high-harmonic spectra, the development of the corresponding algorithm will be the subject of a future analysis.

The influence of laser chirp on high harmonic spectra was studied for 30–100 femtosecond pulses in Refs. [12,13]. In particular, asymmetry in spectral broadening of individual harmonics as a function of the sign of the chirp of the driving pulse was analyzed, showing the compensation of the natural negative chirp of high harmonics by the positive chirp of the driving pulse [12–14]. The role of the incident chirp in extending the harmonic cutoff [15] and spectral smoothing near the cutoff region [16] were also studied. Unfortunately, in Refs. [15,16] the chirp of the driving field was modeled by assuming a time dependence of the carrier frequency, e.g., $\omega(t) = \omega_0 + \beta t$, and thus changing the spectral content of the pulse when changing the chirp parameters. However, in experiments the chirp arises in the frequency domain, keeping the spectral content the same.

II. EXPERIMENTAL RESULTS

In our experiments we used a Ti:sapphire-based laser system with a single stage regenerative amplifier producing 30 fs pulses with up to 3 mJ energy and 795 nm central

*zhavoron@mbi-berlin.de

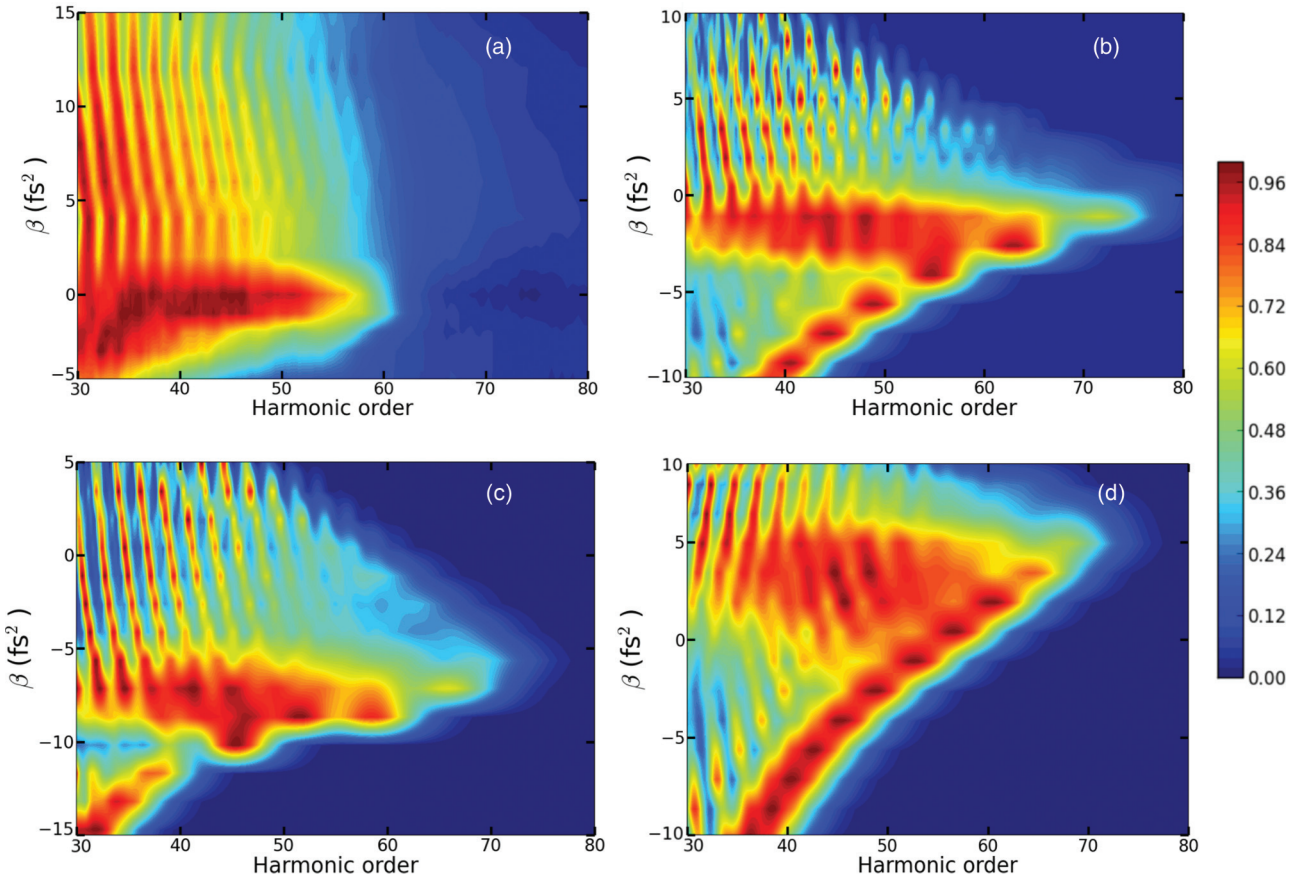

FIG. 1. (a) Experimentally measured HHG spectra for dispersion varying from -5 to 15 fs^2 (HHG D-scan). (b)–(d) Calculated CEP-averaged HHG spectra as a function of second-order dispersion (HHG D-scan) for pulses with uncompensated third-order dispersion: (b) $\gamma_0 = 0$ fs^3, (c) $\gamma_0 = 25$ fs^3, and (d) $\gamma_0 = -25$ fs^3, and the same spectrum as in the experiment. The experimental spectrum in panel (a) was shifted in β so that maximum cutoff occurs at $\beta = 0$. The calculated spectra in panels (b)–(d) were not shifted. Note, for γ different from zero [panels (c) and (d)], the shortest pulse and the highest cutoff are achieved for β different from zero.

wavelength at 1 kHz repetition rate. The CEP of the pulses was not locked. About 1.4 mJ of the output energy was directed into a differentially pumped hollow-core-fiber (HCF) pulse compressor filled with neon. The spectrally broadened pulses at the output of the HCF were compressed with a set of mirrors with negative dispersion (Layertec GmbH). A pair of fused silica wedges (2.4 degree apex) was used to introduce and scan the correcting dispersion, enabling systematic control of spectral phase. The initial pulse characterization was performed with a FC-Spider (APE, Berlin). By increasing the pressure of the supplied gas up to 2500 Torr we were able to compress the output pulses continuously down to 4 ± 0.2 fs, with the Fourier limit of 3.2 fs. The presence of uncompensated third- and higher-order spectral phase is the reason for the deviation of the pulse length duration from its Fourier limit. The main contribution came from the third-order phase of about 20 fs^3: its elimination would have brought the pulse duration down to 3.5 fs.

We separated the central part of the output beam with an energy of 0.6 mJ and focused it at f/100 into a 2.5-mm-long gas cell containing neon. The peak intensity in the focus $\simeq 3.4 \times 10^{14}$ W/cm^2 was estimated from the maximum cutoff value. The gas pressure inside the cell was kept within the 12–15 mbar ($\simeq$10 Torr) range by a PC-based gas-mass-flow controller. The residual gas pressure in the interaction chamber was controlled to be no larger than $P_{\text{rest}} \approx 10^{-3}$ mbar. The sufficiently low gas pressure and the intensity, as well as the low chromatic dispersion of neon for the considered parameters, allowed us to make the conclusion about the insignificance of nonlinear propagation effects and ionization-induced contributions to propagation and phase matching, as well as to neglect the pulse broadening due to dispersion. This conclusion was confirmed by systematic scans of the neon pressure: the two-dimensional (2D) spectrograms presented here are robust with respect to these scans. However, we do take advantage of the well-known phase-matching selection between the long and the short trajectories contributing to the high-harmonic signal (see, e.g., Ref. [17]): setting the focal position 2 mm before the gas target we select the short trajectories in the detected on-axis radiation (the long trajectories phase match off-axis). We also note that the laser confocal parameter was 10 mm, significantly longer than the interaction region.

The generated radiation up to harmonic order 71 was detected with the XUV-spectrometer based on a 1 m toroidal mirror and a 600 grooves/mm plane grating. Since the optical paths from the output of the pulse compressor to the FC-Spider and to the HHG interaction region are different, the input pulse shape at the position of the gas cell differs from that measured by Spider and is not known exactly. Additionally, systematic errors and uncertainty of few-cycle FC-Spider

[18,19], together with dispersion introduced by the FC-Spider setup, will contribute to this difference.

We measured and analyzed the XUV spectra as a function of the dispersion introduced by inserting the fused silica wedges, performing a high-harmonic dispersion scan with the step corresponding to $\beta \sim 1$ fs^2. In Fig. 1(a) we plot the result of the HHG D-scan as a two-dimensional trace. One can make the following key observations:

First, the harmonic cutoff decreases as the wedges are moved out of their optimal position. Indeed, stretching the pulse due to extra dispersion reduces its peak intensity and hence the HHG cutoff. Second, the decrease in the cutoff is strongly asymmetric relative to the sign of β, with a sharper fall for negative β. This behavior is counterintuitive since, for CEP-stable pulses, negative chirps extend the cutoff, in contrast to the present observation. Third, for random CEP, the spectrum is strongly modulated for $\beta > 0$ but remains smooth for $\beta < 0$. This behavior is also counterintuitive, since for CEP-stable pulses the opposite is expected. The last two findings contradict the common wisdom for chirped few-cycle pulses. We now confirm and explain our results below, using theoretical analysis. We also show that the cutoff behavior and the modulation depth allow one to retrieve the second-order and third-order spectral phases, with high accuracy.

III. THEORETICAL DESCRIPTION AND ANALYSIS

A. Assymetry in cutoff of HHG spectrum

To interpret the measurements, we calculate the CEP-averaged harmonic spectra by using the standard method Ref. [20] for hydrogen-like atoms. The electric field of the pulse in the interaction region is described as

$$F(t) \propto \int d\omega \exp\left[-i\omega t + i\phi(\omega)\right] F(\omega) + \text{c.c.},$$
$$\phi(\omega) = \frac{1}{2}\beta(\omega-\omega_0)^2 + \frac{1}{6}\gamma(\omega-\omega_0)^3, \tag{1}$$

where $F(\omega)$ is the real-valued spectral amplitude, ω_0 is the central frequency, $\beta = \beta(z)$ is the second-order phase coefficient, and third-order phase coefficient $\gamma = \gamma_0 + \gamma(z)$ is parameterized by the initial value γ_0 as well as the wedge contribution $\gamma(z)$, where z is the wedge position. For the driving laser field, we have used the experimentally measured spectrum and systematically added quadratic and cubic spectral phases by changing β and $\gamma(z)$.

We computed the HHG D-scan for different values of γ_0 to obtain the best fit to the experiment. Figures 1(b)–1(d) show the calculated HHG D-scans. The experimentally observed asymmetry in the modulation depth of the HHG spectra is well reproduced. Importantly, we find that this counterintuitive behavior of the modulation depth is associated with CEP averaging. For each individual CEP value, negatively chirped few-cycle pulses have somewhat stronger modulation than positively chirped few-cycle pulses. However, the position of the modulation minima is strongly CEP sensitive, in contrast to positively chirped pulses. As a consequence, CEP-averaged results display the counterintuitive behavior.

Hence, the observed modulation strength and asymmetry are determined by the sign and the value of β. However, the cutoff position for $\gamma_0 = 0$ [Fig. 1(b)] is nearly symmetric for $\pm|\beta|$,

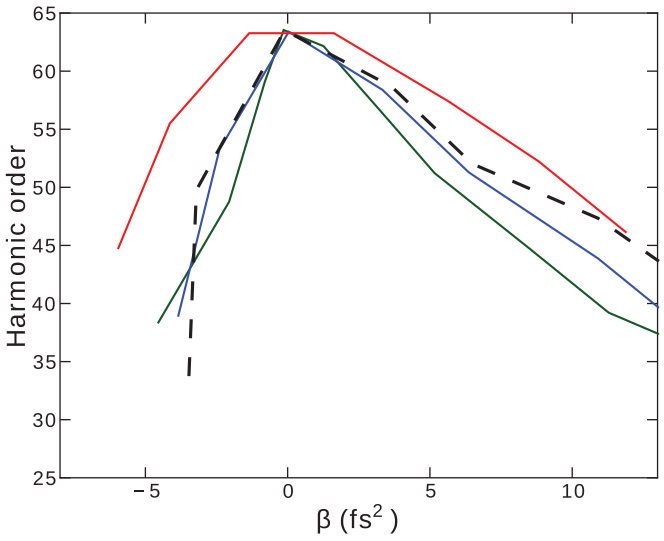

FIG. 2. HHG cutoff vs β. Red, blue, and green corresponds to $\gamma_0 = 40$ fs^3, 25 fs^3, and 12 fs^3, respectively. Experiment is the dashed line.

in contrast with the experiment [Fig. 1(a)], and also in contrast with standard theoretical expectations, especially in view of the previous theoretical works [12,14]. Indeed, for nearly-single-cycle driving pulses, ionization is favored near the pulse peak with the electron returning after the peak. Negative chirp of $\omega(t)$ *in the time domain* increases the return energy $E_r(t) \propto F_0(t)^2/\omega^2(t)$ with the reduced instantaneous frequency $\omega(t)$ after the peak, compensating the drop in the field amplitude $F_0(t)$. In contrast, positive temporal chirp decreases $E_r(t)$ by increasing $\omega(t)$ after the peak, compounding the drop in $F_0(t)$. Thus, the cutoff should fall faster for increasing $\omega(t)$ than for decreasing $\omega(t)$. What is wrong with this argument and why do our results indicate the opposite behavior?

The argument tacitly assumes that the frequency chirp is introduced in the time domain, changing $\omega(t)$ but preserving $F_0(t)$. This, however, is not compatible with experiments because it changes the pulse spectrum. If the chirp is introduced in the frequency domain, as in experiments, the pulse is also stretched. The pulse stretching and the associated drop of intensity play a dominant role in the behavior of $E_r(t)$, leading to symmetry with respect to β. Figure 2 demonstrates that the cutoff asymmetry vs β arises due to uncompensated cubic chirp γ_0. In our calculations, γ_0 was varied from -50 to 50 fs^3 in steps of 5 fs^3. The best agreement between the calculated and measured cutoff dependence is obtained for $\gamma_0 = 25$ fs^3. The corresponding HHG D-scan is shown in Fig. 1(c). Figure 1(d) shows the HHG D-scan for $\gamma_0 = -25$ fs^3, illustrating the HHG D-scan with opposite asymmetry. Substantial deviations from the best fit are clearly visible for $\sim$5 fs^3 deviations from the optimal γ value.

In our case, the shift in the wedge positions required for the highest HHG cutoff amounts to introducing an additional quadratic phase of 7 fs^2 at the gas cell position compared with the position where the Spider measurement is done, with a tolerance of about 2 fs^2.

What is the origin of the cutoff asymmetry? For $\gamma_0 > 10$ fs^3 the pulse develops a satellite, which reduces the intensity of the main pulse and thus the HHG cutoff. The behavior of the

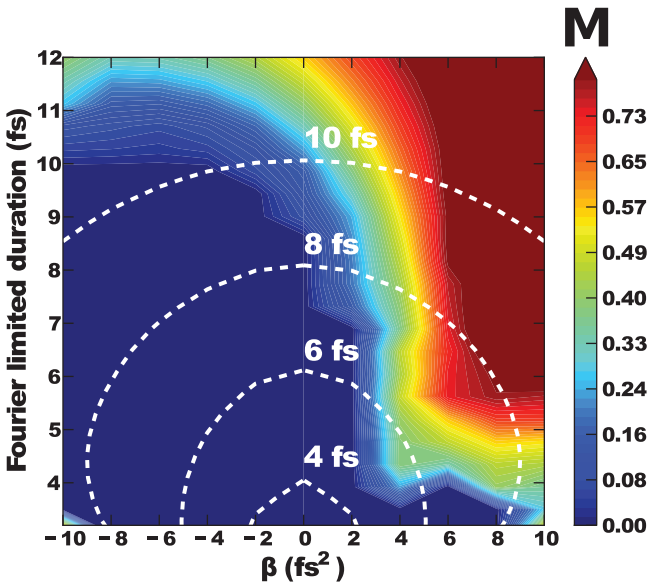

FIG. 3. Modulation depth **M** of the CEP-averaged HHG spectra produced by a pulse with a Gaussian envelope. Dashed white lines shows contours of constant pulse duration vs t_f and β.

satellite pulse vs β is asymmetric: its strength grows rapidly for $\beta < 0$, but slowly for $\beta > 0$. Thus, the main pulse remains more intense for $\beta > 0$. The inverse picture is observed for negative γ_0. Thus, the asymmetry of the cutoff behavior vs β allows us to determine γ_0, here with an accuracy of about 5 fs^3.

B. Modulation depth in HHG spectrum

We now turn to the second key feature of the experimental HHG D-scan: the spectral modulation in Fig. 1. Figures 1(b)–1(d) show that it is independent of γ_0 and is highly asymmetric versus β. The general origin of this effect is the interplay between the intrinsic chirp of the HHG process and the chirp of the laser pulse [14,21]. Figure 3 shows the spectral modulation depth **M** for the CEP-averaged HHG D-scans, calculated for a pulse with a Gaussian spectrum, as a function of its transform-limited duration t_f and the spectral chirp. The modulation depth **M** is defined as $\mathbf{M} = \langle 1 - S_{\min}(N)\rangle / S_{\max}(N)$, where $S_{\min}(N)$ and $S_{\max}(N)$ correspond to the minimum and the maximum of the HHG signal near the harmonic order N in the vicinity of the cutoff. That is, setting for example $N = 51$, we find the maximum and the minimum signal in the window $N = 50$–52. To ensure the stability of the result, additional averaging is performed over a range of harmonic orders $\Delta N \approx 15$. Small $\beta > 0$ already leads to large **M** for pulses with t_f as short as 4 fs. In contrast, for $\beta < 0$ and pulses up to $t_f \simeq 10$ fs, **M** becomes substantial only at the end of the D-scan, in agreement with the experimental data from Fig. 1. The strong asymmetry in the modulation depth **M** as a function of β shows that it can be used to characterize the quadratic phase chirp β_0 in the HHG D-scan.

For few-cycle pulses, the two most important attosecond bursts occur near the field maximum. For a given electron return energy, the relative phase $\Delta\phi(\beta)$ between these bursts dictates the position of the maxima in the spectrum. That is, for zero $\Delta\phi(\beta)$ the maxima will be positioned at odd

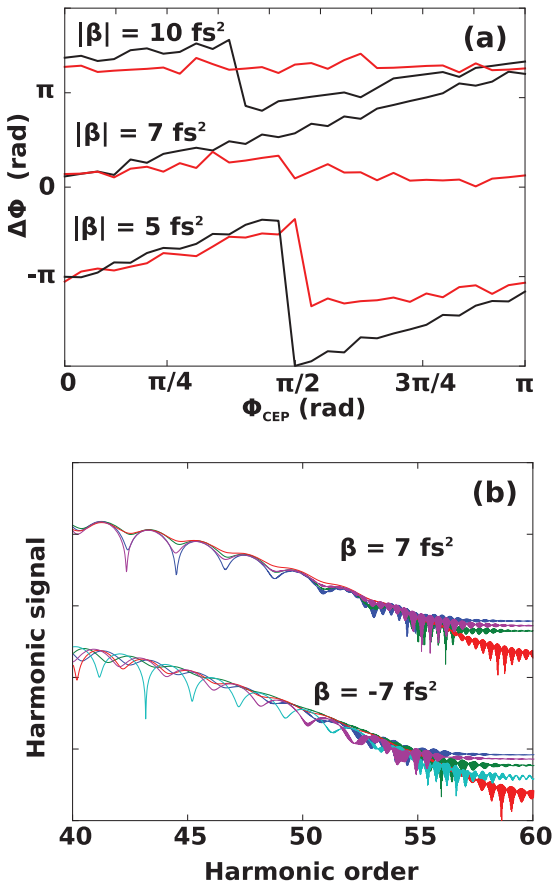

FIG. 4. (a) Relative phase between the two main attosecond bursts for the cutoff harmonics, for different $\beta > 0$ (red) and $\beta < 0$ (black). (b) Theoretical HHG spectra vs CEP, for $|\beta| = 7$ fs^2: $\phi_{CEP} = 0$ (blue), $\pi/3$ (green), $\pi/2$ (red), $3\pi/2$ (purple), and $8\pi/9$ (cyan).

harmonics, as it is typical for long pulses, while for extreme case $\Delta\phi(\beta) = \pi$ the maxima will be at even harmonic numbers (see, e.g., Refs. [1,22] for early work on this subject). For a non-CEP-stabilized pump, if the variation is strong and CEP dependent, the modulations will be averaged out. However, if $\Delta\phi(\beta)$ remains relatively constant with varying CEP, the modulation will persist in the CEP-averaged spectrum.

As shown in Fig. 4(a), the variation of $\Delta\phi(\beta)$ with CEP is much lower for $\beta > 0$ than for $\beta < 0$. This is manifest also in the spectra shown in Fig. 4(b) by constructive summation of different CEP contributions for $\beta = 7$ fs^2 and smoothed CEP-averaged spectrum for $\beta = -7$ fs^2.

We can quantify the impact of the chirp and of the CEP averaging on the spectral modulation depth with an analytical model. The phase of the Nth harmonic is [23]

$$\phi = \mathrm{Re}\left[\frac{1}{2}\int_{t_i}^{t_r} [p_s + A(t')]^2 dt' + I_p(t_r - t_i) - N\omega_0 t_r\right], \quad (2)$$

where I_p is the ionization potential, ω_0 is the laser frequency, t_i, t_r are the ionization and recombination times, and p_s is the electron drift momentum which ensures its return to the atom. Near the cutoff, Eq. (2) yields [24]

$$\phi_{\mathrm{cutoff}}(\omega, I) = -0.94\frac{I_p}{\omega} - 10.17\frac{U_p}{\omega}. \quad (3)$$

For a short chirped pulse, for each laser cycle we use cycle-averaged frequency ω and approximate $A(t)$ by a sine function with frequency ω and amplitude $F_{\max}/\omega$ in this laser cycle. The CEP change can be interpreted as a temporal shift of the bursts while assuming that the quantities $U_p(t)$ and $\omega(t)$ are roughly CEP independent. Just after the pulse peak, where most HHG occurs, the dominant term of the harmonics phase in Eq. (3), $10.17U_p(t)/\omega(t) \sim I(t)/\omega^3(t)$, changes rapidly, when both $I(t)$ and $1/\omega(t)^3$ decrease for $\beta > 0$. In contrast, for $\beta < 0$, the increasing $1/\omega(t)^3$ somewhat compensates the decrease of $I(t)$. Therefore, while changing the CEP will shift the temporal positions of the bursts, maintaining the constant phase between them with $\beta > 0$ will keep the maxima and minima in the HHG spectrum in the same place. In contrast, for $\beta < 0$ the phase difference between adjacent attosecond bursts changes by $\approx 1\pi$, changing the position of the spectral maxima vs CEP by $\sim\omega_0$, leading to smooth CEP-averaged spectra as in Fig. 4(b).

IV. CONCLUSION

In conclusion, we have shown how the HHG D-scan trace can be analyzed to separate the contributions of the second-order and third-order spectral phase. As a part of our analysis, we have experimentally demonstrated and theoretically explained counterintuitive behavior of the harmonic spectrum with the chirp for few-cycle pulses. While it is commonly assumed that negatively chirped few-cycle pulses should lead to better-pronounced, stronger-modulated harmonic spectra, the opposite is true for pulses with unlocked CEP. We also find that, when the frequency chirp is introduced in the spectral rather than the temporal domain, it does not lead to extended cutoff spectra, in contrast with previously published results.

Whereas the asymmetry of the cutoff profiles in the HHG D-scan is caused by the uncompensated γ_0, the sign and the value of β control the modulation in the HHG spectrum in the vicinity of the cutoff. Our modeling confirms the universality of these features for different pulse spectra. Strong sensitivity of the HHG D-scan to minor changes in the dispersion at the level of ≈ 2 fs^2 and ≈ 5 fs^3 open the possibility of using such scans to characterize the pulse directly in the focal region where highly nonlinear interaction takes place. An important feature of HHG D-scan is that spectral phases can be extracted without CEP stabilization, decreasing the technical challenges associated with the implementation of this method. While our present analysis is limited to the second- and third-order spectral phases, we hope that a global fit to the overall two-dimensional HHG spectrum should allow one to extract higher-order spectral phases. Development of the corresponding algorithm is a subject for future work.

ACKNOWLEDGMENTS

M.I., N.Z., and D.B. acknowledge support from the Priority Programm QUTIF (SPP 1840 of Deutsche Forschungsgemeinschaft). N.Z. also acknowledges C. Kleine and U. Bengs for help with running the XUV-spectrometer and Dr. O. Kornilov (MBI) for fruitful discussions.

[1] C. A. Haworth *et al.*, Nat. Phys. **3**, 52 (2007).
[2] L. E. Chipperfield, J. S. Robinson, J. W. G. Tisch, and J. P. Marangos, Phys. Rev. Lett. **102**, 063003 (2009).
[3] E. Goulielmakis, M. Schultze, M. Hofstetter, V. S. Yakovlev, J. Gagnon, M. Uiberacker, A. L. Aquila, E. M. Gullikson, D. T. Attwood, R. Kienberger, F. Krausz, and U. Kleineberg, Science **320**, 1614 (2008).
[4] S. Haessler, T. Balčiunas, G. Fan, G. Andriukaitis, A. Pugžlys, A. Baltuška, T. Witting, R. Squibb, A. Zaïr, J. W. G. Tisch, J. P. Marangos, and L. E. Chipperfield, Phys. Rev. X **4**, 021028 (2014).
[5] L. E. Chipperfield, J. W. Tisch, and J. P. Marangos, J. Mod. Opt. **57**, 992 (2010).
[6] F. Krausz and M. Ivanov, Rev. Mod. Phys. **81**, 163 (2009).
[7] K. T. Kim, C. Zhang, A. D. Shiner, B. E. Schmidt, F. Legare, D. M. Villeneuve, and P. B. Corkum, Nat. Photonics **7**, 958 (2013).
[8] A. S. Wyatt, T. Witting, A. Schiavi, D. Fabris, P. Matia-Hernando, I. A. Wamsley, J. P. Marangos, and W. G. Tisch, Optica **3**, 303 (2016).
[9] P. Carpeggiani, M. Reduzzi, A. Comby, H. Ahmadi, S. Kühn, F. Calegari, M. Nisoli, F. Frassetto, L. Poletto, D. Hoff, J. Ullrich, C. D. Schröter, R. Moshammer, G. G. Paulus, and G. Sansone, Nat. Photonics **11**, 383 (2017).
[10] M. Miranda, C. L. Arnold, T. Fordell, F. Silva, B. Alonso, R. Weigand, A. L'Huillier, and H. Crespo, Opt. Express **20**, 18732 (2012).
[11] L. M. Machado, R. E. Samad, W. de Rossi, and N. D. V. Junior, Opt. Express **20**, 4114 (2012).
[12] D. G. Lee, J.-H. Kim, K.-H. Hong, and C. H. Nam, Phys. Rev. Lett. **87**, 243902 (2001).
[13] Z. Chang, A. Rundquist, H. Wang, I. Christov, H. C. Kapteyn, and M. M. Murnane, Phys. Rev. A **58**, R30(R) (1998).
[14] M. Murakami, J. Mauritsson, and M. B. Gaarde, Phys. Rev. A **72**, 023413 (2005).
[15] J. J. Carrera and S.-I. Chu, Phys. Rev. A **75**, 033807 (2007).
[16] Y. Niu, Y. Xiang, Y. Qi, and S. Gong, Phys. Rev. A **80**, 063818 (2009).
[17] P. Agostini and L. F. DiMauro, Rep. Prog. Phys. **67**, 813 (2004).
[18] A. S. Wyatt, A. Gruen, P. K. Bates, O. Chalus, J. Biegert, and I. A. Walmsley, Opt. Express **19**, 25355 (2011).
[19] R. Trebino, *Frequency-Resolved Optical Gating: The Measurement of Ultrashort Pulses* (Kluwer Academic Publisher, Boston, 2000).
[20] M. Lewenstein, P. Balcou, M. Y. Ivanov, A. L'Huillier, and P. B. Corkum, Phys. Rev. A **49**, 2117 (1994).
[21] R. Bartels, S. Backus, E. Zeek, L. Misoguti, G. Vdovin, I. P. Christov, M. M. Murnane, and H. C. Kapteyn, Nature (London) **406**, 164 (2000).
[22] A. de Bohan, P. Antoine, D. B. Milošević, and B. Piraux, Phys. Rev. Lett. **81**, 1837 (1998).
[23] O. Smirnova and M. Ivanov, in *Attosecond and XUV Physics*, edited by T. Schultz and M. Vrakking (Wiley-VCH Verlag GmbH & Co. KGaA, Berlin, 2014), Chap. 7, pp. 201–256.
[24] M. A. Khokhlova and V. V. Strelkov, Phys. Rev. A **93**, 043416 (2016).